International Journal of Precision Engineering and Manufacturing-Green Technology (2024) 11:1217–1228
https://doi.org/10.1007/s40684-023-00577-6

Online ISSN 2198-0810
Print ISSN 2288-6206

REGULAR PAPER

Evaluation of Electrolyte Materials of Gd- and Ce-Doped Scandia-Stabilized Zirconia and Yb- and Bi-Doped Gadolinium-Doped Ceria for Highly Durable Solid Oxide Fuel Cells

Sanghun Lee[1] · Kunho Lee[2] · Jaemyung Lee[3] · Jaeseok Lee[3] · Taehong Kim[3] · Joongmyeon Bae[3]

Received: 28 February 2023 / Revised: 10 October 2023 / Accepted: 18 October 2023 / Published online: 30 November 2023

Abstract

Solid oxide fuel cells (SOFCs) have attracted significant attention as a highly efficient type of fuel cell. Recent research proposes the use of co-doped scandium-stabilized zirconia with Gd and Ce (denoted as 10Sc0.5Gd0.5CeSZ) and Yb and Bi co-doped gadolinium-doped ceria (denoted as GYBC) as promising materials for the electrolyte and buffer layers, respectively. 10Sc0.5Gd0.5CeSZ exhibits excellent structural stability and ionic conductivity, which can be attributed to the doping of Ce for enhanced stability and Gd for improved ionic conductivity. On the other hand, GYBC demonstrates good sinterability and ionic conductivity due to the ability of Bi to lower the sintering temperature and the high ionic conductivity of Yb. To evaluate the feasibility of 10Sc0.5Gd0.5CeSZ and GYBC at the single cell level. X-ray diffraction (XRD) peaks and Rietveld refinements show good structural stability with slight increase in the lattice parameter by doping. The particle morphologies, size distributions, and BET surface areas are evaluated for the basic material characterizations. Then, lanthanum strontium cobalt ferrite (LSCF)–gadolinium-doped ceria (GDC) was selected as cathode material with 10Sc0.5Gd0.5CeSZ and GYBC. Finally, a single cell composed of Ni-Yttria stabilized zirconia (YSZ)/10Sc0.5Gd0.5CeSZ/GYBC/LSCF-GDC (6.5:3.5) is fabricated by sequential 3-layer co-tape casting technique, and it shows good open circuit voltage of > 1.0 V, high electrochemical performance of 0.73 W/cm^2 and low ohmic resistance of 0.17 Ωcm^2 at 750 °C. Then, the electrochemical characteristics and long-term durability of this single cell are evaluated over 500 h without degradation issues. Based on these results, it is concluded that 10Sc0.5Gd0.5CeSZ and GYBC are promising candidate materials for SOFCs.

Keywords Solid oxide fuel cell · Electrolyte · Buffer layer · Tape casting · Durability

1 Introduction

A solid oxide fuel cell (SOFC) is a high temperature fuel cell that is composed of ceramic materials, and it has attracted attention because of the various advantages [1–6]. Because of the high SOFC operating temperature of 500–850 °C, low cost perovskite-structured electrodes instead of noble metals such as platinum can be used for SOFCs, which improves economic competitiveness of the fuel cells [7, 8]. High temperature waste heat from SOFCs can be also utilized for heating. In addition, SOFCs can be operated at higher efficiencies than low temperature fuel cells such as polymer electrolyte membrane fuel cells (PEMFCs) and phosphoric acid fuel cells (PAFCs) [9, 10]. Various hydrocarbon fuels can be used directly as fuel for SOFCs [11]. For these advantages, SOFCs have been studied for various power generation systems [12–14].

Sanghun Lee and Kunho Lee have the Co-first authors.

✉ Sanghun Lee
sanghun@ewha.ac.kr

✉ Joongmyeon Bae
jmbae@kaist.ac.kr

[1] Department of Climate and Energy Systems Engineering, Ewha Womans University, 52, Ewhayeodae-gil, Seodaemun-gu, Seoul, Republic of Korea

[2] Research and Development Center, Saudi Aramco, 31311 Dhahran, Saudi Arabia

[3] Department of Mechanical Engineering, Korea Advanced Institute of Science and Technology (KAIST), 291 Daehak-ro, Yuseong-gu, Daejeon 305-701, Republic of Korea

However, the high operating temperature of SOFCs have limited the metallic components used for SOFC stacks, and reduce the long-term durability by coarsening of Ni particles at anodes, oxidation of metallic components, and chromium poisoning issues of cathodes [15, 16]. To solve these issues, continuous efforts to reduce the operating temperature of SOFCs have been reported [17]. However, ionic conductivities of the electrolyte materials decrease as the operating temperatures decrease, which reduces electrochemical performance of the SOFCs. For the low temperature operation of SOFCs, electrolyte materials with high ionic conductivities even at low operating temperatures such as Lanthanum strontium gallium magnesium oxide (LSGM), Scandia-stabilized Zirconia (ScSZ), and Ceria and Yttria doped Barium Zirconate (BZCY) have been developed [18–20]. ScSZ is one of the promising electrolyte materials that can be used for low temperature operation of SOFCs because of its high ionic conductivity and low activation energy for the movement of oxygen ions [21–23].

However, ScSZ has a limitation of low structural stability such as phase transition from cubic to rhombohedral or tetragonal phase depending on the amount of dopants or temperature, and aging issues caused by long-term exposure to SOFC operating temperatures [24–26]. To solve these issues, various materials such as Ce, Ti, Bi, and Y are doped into ScSZ [27–30]. However, doped ScSZ still has degradation issues due to the increased grain boundary resistance caused by the gradual diffusion of cations such as Ce^{3+} from the inside of grain to the grain boundary [31, 32]. Recently, Ce- and Yb, Gd, or Sm co-doped ScSZ have been proposed to improve the stability of doped ScSZ materials by reducing the amount of diffusing cations of Ce^{3+} by substituting them with other more stable cations [26, 33]. Ce- and Gd-co doped ScSZ showed excellent structural stability and high ionic conductivity compared to Ce-doped ScSZ, Sm, Ce co-doped and Yb, Ce co-doped ScSZ [26].

To fabricate single cells with high electrochemical performances, highly active cathode materials are required. Lanthanum strontium cobalt ferrite (LSCF) is one of the most frequently used cathode materials for SOFCs [34–36]. However, LSCF reacts with doped zirconia electrolytes such as yttria-stabilized zirconia (YSZ) and doped-ScSZ, forming secondary phases of strontium zirconate ($SrZrO_3$) and lanthanum zirconate ($La_2Zr_2O_7$) at the interface when it is sintered and operated at high temperatures above 900 °C [37–39]. To prevent these side reactions, dense buffer layers composed of ceria-based materials such as gadolinium-doped ceria (GDC) can be deposited between LSCF and doped-ScSZ [23, 40]. However, there are following issues to fabricate the dense buffer layers: 1. High sintering temperature of 1350–1600 °C required for GDC, and 2. Constrained sintering of buffer layers on pre-sintered electrolyte which prevent full densification of the buffer layer [41]. To solve these issues, Bi-doped GDC is proposed to reduce the sintering temperature through transient liquid phase-assisting mechanism [42]. By doping Bi into GDC, the sintering temperature can be reduced to 1200–1400 °C. However, the ionic conductivity of the Bi-doped GDC is also reduced because of a larger cation radius of Bi of 0.1170 nm than Gd of 0.1053 nm, narrowing oxygen ion diffusion path [43, 44]. For this reason, Yb- and Bi- co doped GDC is proposed by substituting a portion of Bi with Yb, which has a cation radius of 0.0985 nm, leading to higher ionic conductivity [44].

Ce- and Gd-co doped ScSZ (10Sc0.5Gd0.5CeSZ) and Yb- and Bi- co doped GDC (GYBC) have been studied as a potential electrolyte and buffer layers for SOFCs due to their higher structural stability, ionic conductivity, and good sinterability than the conventional ScSZ and GDC. 10Sc0.5Gd0.5CeSZ has higher structural stability and ionic conductivity by doping Ce for the strong stability and Gd for the high ionic conductivity. GYBC has higher sinterability and ionic conductivity by doping Bi for lowering sintering temperature and Yb for high ionic conductivity Previous studies have mainly focused on the basic feasibility study on the materials properties such as materials synthesis, composition screening, crystal structure, and conductivity measurement [26, 33, 44]. However, the processability, sinterability, and durability have not been reported, which are significant for the commercialization of the electrolyte and buffer layer materials for SOFCs.

In this study, comprehensive analyses including material characterization, cell fabrication using mass production techniques, electrochemical characterization, and long-term testing were conducted to further assess the viability of 10Sc0.5Gd0.5CeSZ and GYBC at the single-cell level, which has not been reported before. The material characteristics of 10Sc0.5Gd0.5CeSZ and GYBC were investigated through X-ray diffraction (XRD) with Rietveld refinement, BET surface area measurements using N_2 physisorption, and observation of powder morphologies using transmission electron microscopy (TEM) images and image processing techniques. Subsequently, LSCF-GDC cathodes with ratios of 6.5:3.5 and 6:4 were evaluated with sintering temperatures of 1100 °C and 1050 °C to optimize the fabrication conditions when used on a doped ceria layer. Investigations included XRD, microstructural analysis through scanning electron microscopy (SEM) and image processing, BET surface area measurements using N_2 physisorption, and electrochemical impedance spectra (EIS). Following these evaluations, a single cell was fabricated using the sequential 3-layer co-tape casting process, which allows the sequential coating and simultaneous sintering of the anode support, anode functional layer, and electrolyte. The single cell was composed of Ni-YSZ anode support/Ni-YSZ anode functional layer/10Sc0.5Gd0.5CeSZ electrolyte/GYBC buffer

layer/LSCF-GDC (6.5:3.5) cathode. The electrochemical performance and EIS of the produced single cell were thoroughly evaluated, and the durability of the single cell was tested for 500 h to assess its long-term stability and reliability.

2 Experimental

2.1 Characterization of Materials Properties

In this study, the electrolyte materials used were Ce- and Gd-co-doped ScSZ with the chemical formula $(Sc_2O_3)_{0.1}(Gd_2O_3)_{0.005}(CeO_2)_{0.005}(ZrO_2)_{0.89}$, referred to as 10Sc0.5Gd0.5CeSZ, and Yb- and Bi-co-doped GDC with the chemical formula $(Gd_2O_3)_{0.0675}(Yb_2O_3)_{0.0075}(Bi_2O_3)_{0.01}(CeO_2)_{0.83}$, denoted as GYBC. The cathodes used were LSCF-GDC with a weight ratio of 6:4 and 6.5:3.5, comprising $La_{0.6}Sr_{0.4}Co_{0.3}Fe_{0.7}O_{3-\delta}$ (LSCF6437) and $Gd_{0.1}Ce_{0.9}O_{1.95}$, which were prepared by Kceracell (South Korea). To observe the morphologies of the materials, SEM (FE-SEM S-4300, Hitachi, Japan) and transmission electron microscope-energy dispersive spectroscopy (TEM-EDS, JEM-ARM200F, JEOL, Japan) were utilized. The Brunauer–Emmett–Teller (BET) surface areas and corresponding particle sizes were determined through N_2 physisorption (3Flex, Micromeritics, USA), assuming no particle agglomeration and spherical particle shapes. Particle size distributions of 10Sc0.5Gd0.5CeSZ and GYBC, as well as the porosities of the LSCF-GDC electrodes, were assessed through TEM and SEM image processing, respectively, using ImageJ software. To investigate the crystalline structures, XRD analysis (SmartLab X-ray diffractometer, Rigaku, Japan) was carried out. The lattice parameters and cell volumes were then analyzed through Rietveld refinement using Highscore Plus software.

2.2 Electrochemical Impedance Spectrometry (EIS) Analysis on LSCF-GDC Cathodes

Symmetrical cells were prepared to assess the EIS of LSCF-GDC cathodes at various sintering temperatures and weight ratios. GDC electrolyte pellets with a diameter of 2 cm and a thickness of 0.100 cm were fabricated using the dry-pressing method and sintered at 1450 °C for 6 h. For the cathodes, pastes were prepared by mixing LSCF-GDC powders in weight ratios of 6:4 and 6.5:3.5 with a terpineol-based ink vehicle using magnetic stirring. These cathode pastes were then coated on both sides of the GDC electrolyte pellets using the screen printing method and sintered at 1050 °C and 1100 °C for 2 h.

The prepared symmetrical cells were subjected to testing at temperatures ranging from 650 to 800 °C with intervals of 50 °C. For the alternating current (AC) impedance measurements, air was supplied at a rate of 300 standard cubic centimeters per minute (sccm) (SI 1260, SI 1287, Solartron, UK). A four-probe method was used to minimize the effects of ohmic resistance caused by current-collecting wires. The measured frequency range was from 0.05 to 10^6 Hz, and an applied voltage amplitude of 20 mV was used during the experiments.

2.3 Fabrication and Electrochemical Performance Test on Single Cells

To fabricate single cells with a 10Sc0.5Gd0.5CeSZ electrolyte, a cost-effective manufacturing technique for SOFCs known as the sequential 3-layer co-tape casting technique was established. The process consists of four main steps, as illustrated in Fig. 1: ink preparation, de-airing, coating & drying, and heat treatment. The composition of the tape cast slurries used for the electrolyte, anode functional layer (AFL), and anode support can be found in Table 1. First, 10Sc0.5Gd0.5CeSZ tapes were fabricated by the tape casting

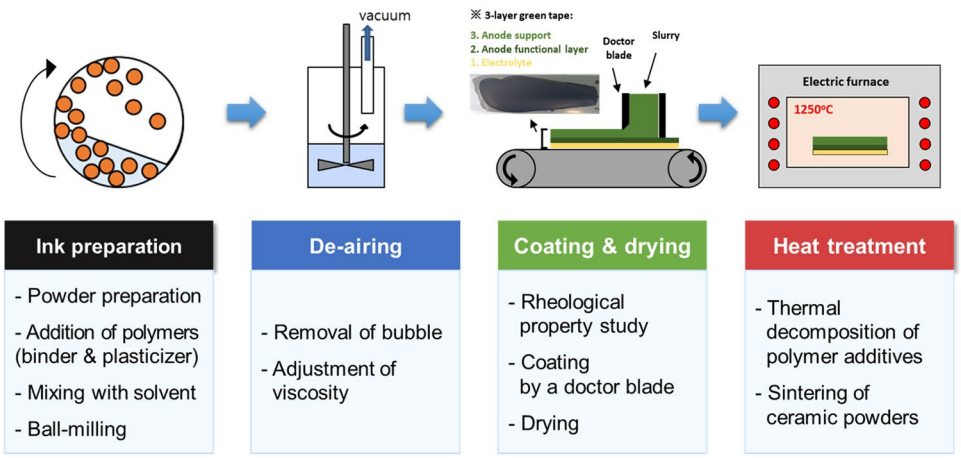

Fig. 1 Single cell fabrication process using a sequential 3-layer co-tape casting technique

Table 1 Compositions of tape cast slurries for electrolyte, AFL, and anode support

Powder					Solvent		Dispersant	Binder	Plasticizer	
Materials	NiO [Kcera-cell]	YSZ [TOSOH]	10Sc0.5Gd0.5CeSZ [Kceracell]	Carbon black	Toluene	Ethanol	Triton	Polyvinyl Butyral (PVB 79)	Benzyl Butyl Phthalate (BBP)	Polyethylene Glycol (PEG 8000)
Weight [g]										
Electrolyte	–	–	67	–	21	21	2	6.75	5.25	1.5
Anode functional layer	42	25	–	–	21	21	2	6.75	5.25	1.5
Anode support layer	42	25	–	6.7	21	33	3	8.8	6.9	2.0

technique. Ink formulation such as powder loading, binder and plasticity ratio for 10Sc0.5Gd0.5CeSZ was determined as the same formulation with ScSZ because the measured BET surface area of 10Sc0.5Gd0.5CeSZ and ScSZ were on a similar level. Subsequently, AFL and anode support tapes were cast over the prepared electrolyte. These 3-layer tapes, comprising the anode support, AFL, and electrolyte, were then cut into coin-sized pieces with a diameter of 2.5 cm, and co-sintered at a temperature of 1250 °C for 4 h. Densification of 10Sc0.5Gd0.5CeSZ electrolyte was successfully conducted with the shrinkage of underlying anode support and AFL. The detailed procedures for the 3-layer co-tape casting can be found in a previous study [34]. For the coating of buffer layer, GYBC buffer layer coating paste was prepared by mixing with terpineol ink vehicle, and it was coated on the electrolyte by spin coating method with a 4,000 rpm under the pre-set standard conditions. The GYBC buffer layer was sintered at a temperature of 1,200 °C for 2 h. For the cathode, a paste consisting of LSCF-GDC (in a 6.5:3.5 weight ratio) was prepared, coated on the buffer layer, and sintered at 1050 °C for 2 h.

The fabricated single cell was evaluated at an operating temperature of 750 °C, utilizing 200 sccm of humidified hydrogen and 300 sccm of air as the gas supply. For the current collection on both sides of the cell, Pt current collecting paste, mesh, and wires were utilized. A current–voltage (I-V) curve was generated to assess the current and voltage characteristics of the cell and AC impedance measurements were performed (SI 1260, SI1287, Solartron, UK). The four-probe method was used for these electrochemical tests. Furthermore, the durability of the single cell was tested for approximately 500 h through galvanostatic operation at a current density of 1 A/cm^2.

3 Results and Discussion

3.1 Materials Properties of 10Sc0.5Gd0.5CeSZ and GYBC

Figure 2 shows the XRD peaks of 10Sc0.5Gd0.5CeSZ and GYBC. Previous reports on the XRD peaks of these materials are scarce [26, 44], but they can also be compared with those of ScSZ and GDC. 10Sc0.5Gd0.5CeSZ is a material in which small amounts of Gd and Ce are doped into ScSZ, while GYBC is a material with small amounts of Yb and Bi doped into GDC. The XRD analysis revealed that there were no distinct Gd, Ce, Yb, and Bi peaks in both materials, indicating the successful incorporation of dopants into the crystalline structure, forming single crystalline phases. However, it is possible that undoped peaks were not observed due to the limited amount of dopants present.

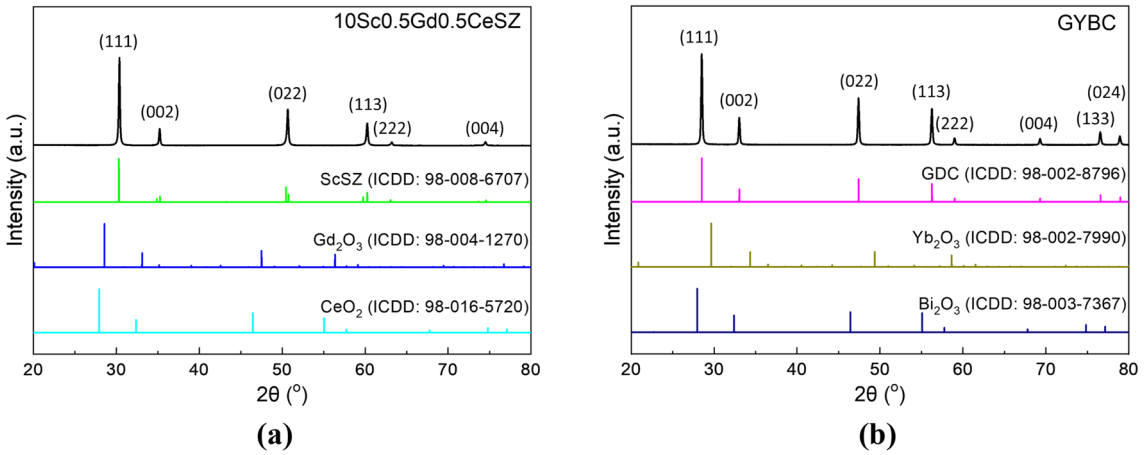

Fig. 2 XRD peaks of **a** 10Sc0.5Gd0.5CeSZ and **b** GYBC

Table 2 Crystallographic data for 10Sc0.5Gd0.5CeSZ and GYBC obtained by Rietveld refinement

Powder	10Sc0.5Gd0.5CeSZ	GYBC
Crystal system	Cubic	Cubic
Space group	$Fm\bar{3}m$	$Fm\bar{3}m$
Lattice parameter (Å)	5.0919	5.4233
Volume $(Å)^3$	132.0163	159.5028

To further investigate the lattice parameters, Rietveld refinement was conducted for both materials, and the results are listed in Table 2. 10Sc0.5Gd0.5CeSZ exhibited a cubic structure with a space group of $Fm\bar{3}m$, which is the same as ScSZ. The lattice parameter of 10Sc0.5Gd0.5CeSZ was 5.0919 Å, slightly larger than the lattice parameter of ScSZ at 5.0910 Å [45]. The additional dopants, Gd^{3+}, Ce^{3+}, and Ce^{4+} cations, have larger radii (1.05 Å, 1.14 Å, and 0.97 Å, respectively) compared to Sc^{3+} and Zr^{4+} with radii of 0.75 Å and 0.74 Å [46–49]. The presence of these larger dopants in 10Sc0.5Gd0.5CeSZ could account for the slightly increased lattice parameters compared to ScSZ. Similarly, GYBC also exhibited a cubic structure with a space group of $Fm\bar{3}m$, matching GDC. The lattice parameter of GYBC was 5.4233 Å, slightly larger than that of GDC at 5.4177 Å [50, 51]. This difference could be attributed to the larger sizes of the Yb^{3+} and Bi^{3+} cations (with radii of 0.96 Å and 1.17 Å, respectively) compared to Gd^{3+}, Ce^{3+}, and Ce^{4+} cations [43]. It is evident from the analysis that 10Sc0.5Gd0.5CeSZ offers improved structural stability and durability, while GYBC achieves lower sintering temperatures and higher ionic conductivity through the doping of Gd and Ce, as well as Yb and Bi, respectively, with only slight increases in the lattice parameters.

Figure 3 presents TEM images of 10Sc0.5Gd0.5CeSZ and GYBC powders, revealing that 10Sc0.5Gd0.5CeSZ exhibited larger particle sizes compared to GYBC. Further analysis of particle sizes was performed using TEM images, as shown in Fig. 4, resulting in average particle sizes of 68.7 ± 12.8 nm for 10Sc0.5Gd0.5CeSZ and 47.3 ± 10.7 nm for GYBC. The d-spacing values, obtained from TEM images and FFT, indicated that both materials exhibited d-spacing values of 2.94 Å and 3.14 Å corresponding to (111) planes. Additionally, the BET surface areas and corresponding particle sizes of 10Sc0.5Gd0.5CeSZ and GYBC were evaluated, as shown in Table 3. The BET surface areas were determined to be 9.7271 m^2/g for 10Sc0.5Gd0.5CeSZ and 10.5517 m^2/g for GYBC, which corresponded to the particle sizes of 104.726 nm and 78.9762 nm, respectively. It is worth noting that the calculated particle sizes were larger than those obtained from the TEM image analysis. This discrepancy could be attributed to the assumptions made in the calculation method, namely the assumptions of no particle agglomeration and particles being perfectly spherical.

3.2 Electrochemical Characterization of LSCF-GDC Electrodes

LSCF is a widely used cathode material due to its mixed ionic and electronic conductor (MIEC) properties, offering high ionic conductivity and excellent electrochemical activity [52–56]. To further increase the electrochemical performance when using LSCF as cathode, LSCF-GDC composite materials are widely used instead of pure LSCF cathode [57]. By using LSCF-GDC composite cathode, ionic conductivity of the cathode can be more increased, resulting in more reaction sites. For this reason, LSCF-GDC was chosen as the cathode material to investigate the performance of 10Sc0.5Gd0.5CeSZ and GYBC at the single-cell level. The structural and electrochemical properties were characterized based on various LSCF:GDC ratios and sintering temperatures. However, because the

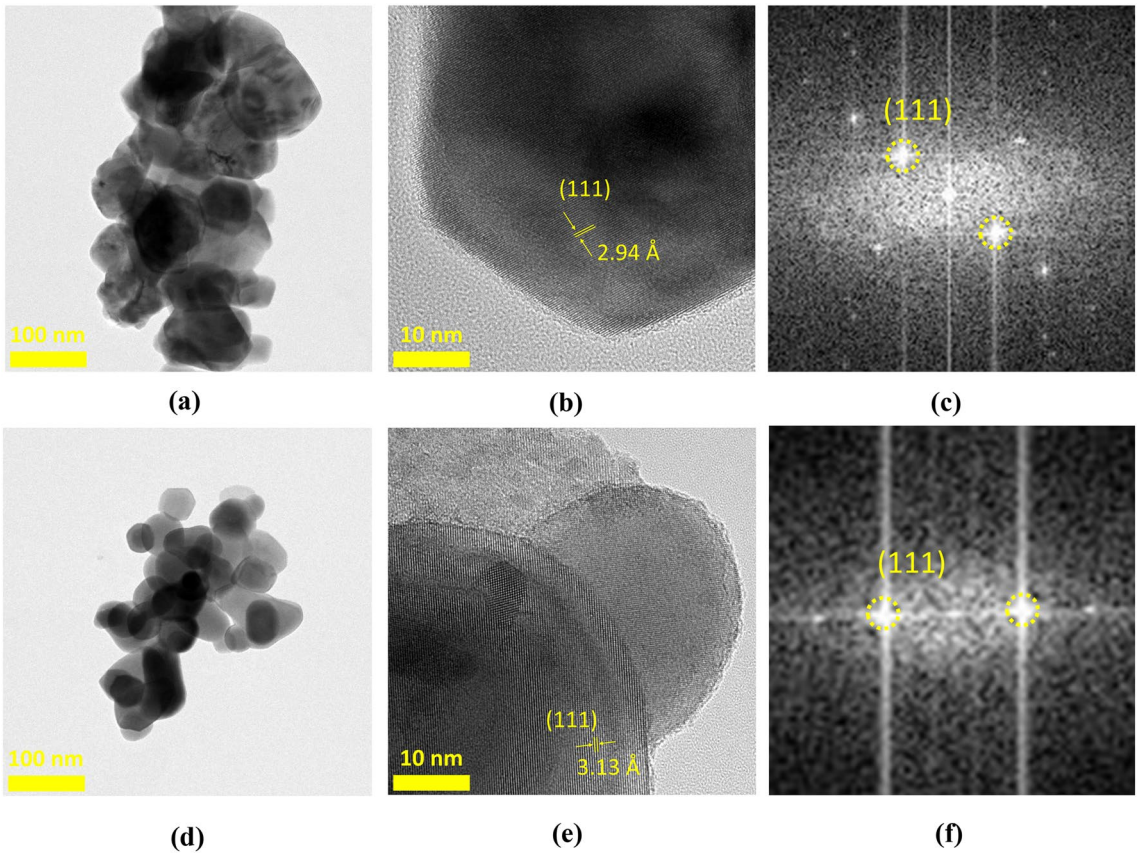

Fig. 3 TEM images of **a**, **b** 10Sc0.5Gd0.5CeSZ and **d**, **e** GYBC, and FFT of (**c**) 10Sc0.5Gd0.5CeSZ and **f** GYBC

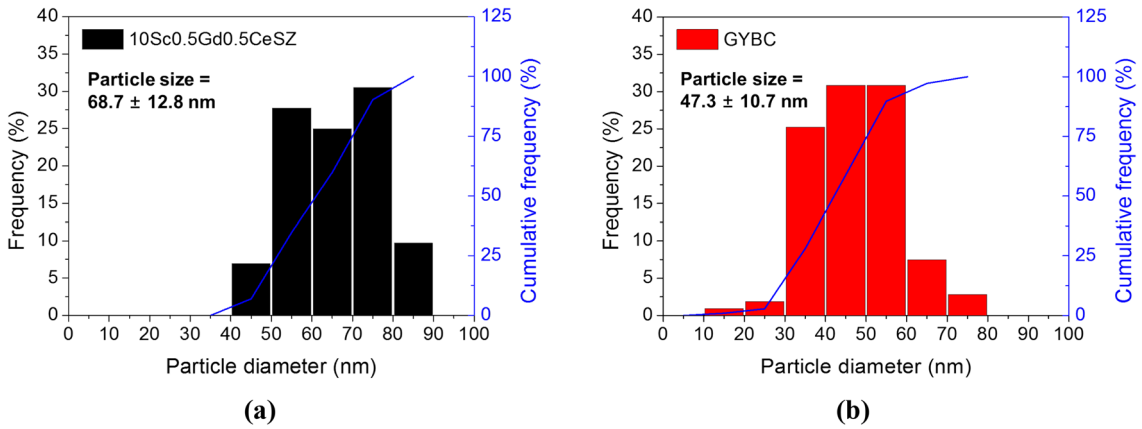

Fig. 4 Particle size distribution of **a** 10Sc0.5Gd0.5CeSZ and **b** GYBC

Table 3 BET surface areas of 10Sc0.5Gd0.5CeSZ and GYBC

Materials	10Sc0.5Gd0.5CeSZ	GYBC
BET surface areas (m^2/g)	9.7271	10.5517
Particle size calculated from BET (nm)	104.726	78.9762

main focus of this study is the feasibility evaluation of 10Sc0.5Gd0.5CeSZ and GYBC electrolyte and buffer layer materials, detailed results can be found in the supplementary material.

3.3 Electrochemical Performance of Ni-YSZ/10Sc0.5Gd0.5CeSZ/GYBC/LSCF-GDC Single Cell

A single cell comprising Ni-YSZ/10Sc0.5Gd0.5CeSZ/GYBC/LSCF-GDC was successfully fabricated using the sequential 3-layer co-tape casting technique. Figure 5(a) illustrates the cross-sectional view of the fabricated single cell. A porous anode support layer of approximately 300 µm, consisting of NiO-YSZ, was formed, with a porosity of 11.5 vol%, consistent with a previous study [34]. A denser AFL layer of 23.5 µm, also composed of NiO-YSZ, was observed on the anode support layer. The AFL was intentionally made dense by excluding pore formers, such as carbon black used in the anode support layer, resulting in the formation of micro-pores necessary for gas diffusion during the reduction of NiO to Ni, which reduces the NiO volume by 40 vol% [58, 59]. A dense electrolyte layer of 10Sc0.5Gd0.5CeSZ, with a thickness of 11 µm, was achieved during the co-sintering process of the anode support, AFL, and electrolyte tapes. This successful formation of a dense electrolyte is noteworthy, as it is often challenging to achieve dense electrolyte layers due to constrained sintering conditions [60, 61]. However, during the co-sintering process of the 3-layer tapes, all the layers of anode support, AFL, and electrolyte sintered and shrank together, resulting in completely dense electrolyte layers without constrained sintering issues. Additionally, a 2 µm thick GYBC buffer layer was successfully formed on the pre-sintered 10Sc0.5Gd0.5CeSZ electrolyte at a low sintering temperature of 1200 °C, made possible by the doping of Bi into the doped ceria. Finally, an 11.5 µm thick LSCF-GDC (6.5:3.5) cathode was formed on the GYBC buffer layer at 1050 °C without any delamination issues.

Figure 5(b) displays the I–V curve of the single cell at an operating temperature of 750 °C, achieving an open circuit voltage (OCV) exceeding 1.0 V, as expected from the presence of a dense electrolyte observed in the SEM image. The maximum power density of the cell reached approximately 0.73 W/cm^2. For EIS analysis, a Nyquist plot was obtained as shown in Fig. 5(c). An ohmic resistance of 0.17 Ωcm^2 was observed, attributed to the electrolyte resistance during ionic

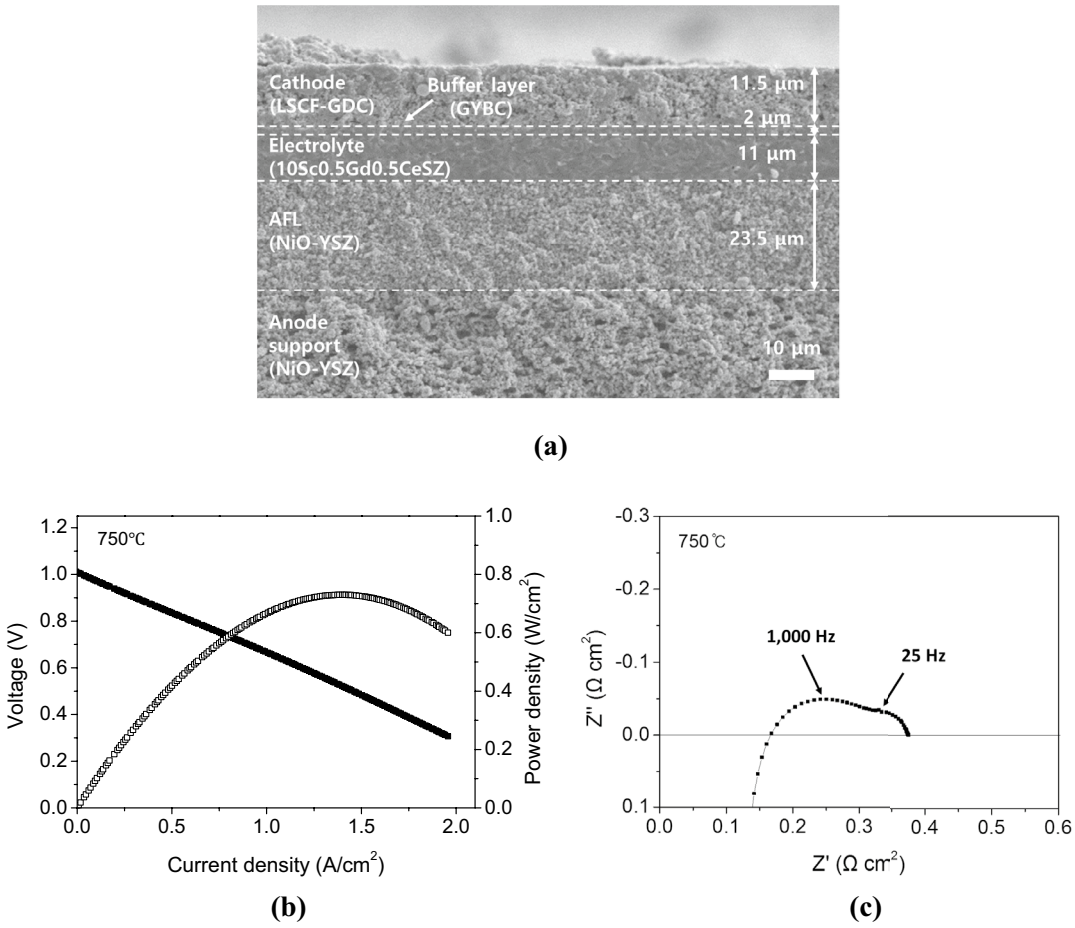

Fig. 5 **a** Cross-sectional SEM image, **b** current–voltage curve, and **c** electrochemical impedance spectrum of the single cell composed of Ni-YSZ/10Sc0.5Gd0.5CeSZ/GYBC/LSCF-GDC (6.5:3.5)

conduction. The impedance spectrum displayed two semicircles with peak frequencies at 1000 Hz and 25 Hz, each representing anode and cathode polarization resistances, respectively. The total polarization resistance caused by the anode and cathode was 0.21 Ωcm^2.

3.4 Durability of Ni-YSZ/10Sc0.5Gd0.5CeSZ/GYBC/LSCF-GDC Button Cells

To ensure the commercial viability of electrolyte and buffer layer materials for SOFCs, assessing their long-term durability is crucial. Electrolyte materials must possess robust crystalline structural stability and high ionic conductivity, while buffer layer materials require high structural stability, high ionic conductivity, and non-reactivity with cathode and electrolyte materials. In this study, the long-term durability of a single cell consisting of 10Sc0.5Gd0.5CeSZ electrolyte and GYBC buffer layer was tested, as shown in Fig. 6.

The single cell exhibited successful operation for 500 h without experiencing any degradation issues. During the initial phase, the operating voltage of the cell gradually increased, leading to higher power density. Then, the operating voltage became constant from 100 h of operation. Several factors could contribute to this increase. The galvanostatic operation during the initial phase could improve the current flowing path of the LSCF-GDC cathode through conditioning (or activation) [62, 63]. Additionally, the use of a small amount of Pt paste for current collection between the cathode and current mesh might have slightly enhanced the electrochemical performance of the LSCF-GDC cathode by depositing Pt particles at its active sites [64]. Subsequently, the operating voltage stabilized and remained constant from 100 h of operation. This steady voltage performance can be attributed to the 1. excellent structural stability and durability of the 10Sc0.5Gd0.5CeSZ electrolyte, along with 2. minimized degradation of LSCF-GDC through the insertion of the dense GYBC buffer layer.

The overall durability of the single cell comprising 10Sc0.5Gd0.5CeSZ and GYBC was found to surpass previously reported single cells using conventional ScSZ electrolyte and GDC buffer layer [22, 26, 65, 66]. This result validates the feasibility of utilizing 10Sc0.5Gd0.5CeSZ and GYBC as SOFC electrolyte and buffer layer materials, respectively, with excellent long-term durability. Nonetheless, further studies should investigate more detailed changes in material properties, microstructures, crystallinities, and interfaces during extended operation to gain a comprehensive understanding of the behavior of the materials.

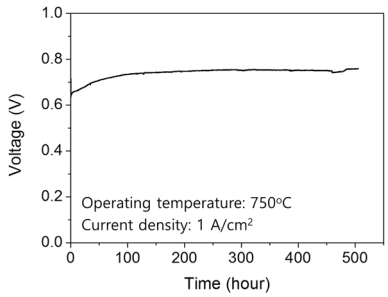

Fig. 6 Galvanostatic long-term durability result of a single cell composed of Ni-YSZ/10Sc0.5Gd0.5CeSZ/GYBC/LSCF-GDC (6.5:3.5)

3.5 Implications and Limitations

In this study, electrolyte and buffer layer materials of 10Sc0.5Gd0.5CeSZ and GYBC were evaluated to be used for SOFCs. As a result, basic materials properties were successfully characterized in terms of crystalline structures by XRD peaks, lattice parameters by Rietveld refinement, BET surface areas, and powder morphologies by TEM images. Also, processabilities were evaluated using 3-layer co-tape casting and spin coating technique with dense electrolyte and no defects, then feasibility of the materials was evaluated on a single cell level with OCV of > 1 V, high electrochemical performance of 0.73 W/cm^2 and ohmic resistance of 0.17 Ωcm^2 by EIS, and durability for 500 h. It is believed that this research is meaningful in terms of proposing new electrolyte materials for SOFCs by doping. However, because it is an early stage work on the new materials, there are some limitations in this work.

First, more detailed electrochemical analyses have to be conducted to evaluate the electrolyte and buffer layer materials of 10Sc0.5Gd0.5CeSZ and GYBC. The properties and performances of the electrolyte and buffer layer materials can be different depending on the sintering, measurement temperature, and interaction between electrolyte, buffer layer, and cathode. Therefore, more detailed analyses such as impedance analysis, DRT, bode plot discussion, and comparison between cells with different configuration, e.g. single cells with and without buffer layer, have to conducted.

Second, the increase of cell voltage during the first 100 h in the long-term stability test have to be further evaluated. As discussed in the previous session, Pt deposition from the current collection mesh to cathode material could improve the performance of the cathode [64]. It is a still very interesting phenomenon and it have to be further explored by experiments and post-mortem analysis only for investigating the phenomenon. Then, the activation of LSCF-GDC by Pt deposition can be verified.

Third, to demonstrate the feasibility of the electrolyte layers more effectively, it is necessary to compare the characteristics and performance of 10Sc0.5Gd0.5CeSZ and GYBC with other electrolyte materials. Then, the possible reasons of the difference have to be further studied. However, as an early stage research, this study only showed the possibility of 10Sc0.5Gd0.5CeSZ and GYBC materials as electrolyte

and buffer layer materials. In addition, interaction between electrolyte materials of 10Sc0.5Gd0.5CeSZ, GYBC, and cathode materials such as pure LSCF, LSCF-GDC composite material have to investigated to evaluate the total compatibility of 10Sc0.5Gd0.5CeSZ and GYBC under the more systematically designed experiments.

4 Conclusion

In this study, we investigated the potential of 10Sc0.5Gd0.5CeSZ and GYBC as electrolyte and buffer layer materials for SOFCs at the single-cell level, which had not been previously reported. The XRD analysis confirmed that 10Sc0.5Gd0.5CeSZ and GYBC exhibited single crystalline phases, indicating the successful doping of Gd, Ce, Yb, and Bi into the crystalline structures of ScSZ and GDC. The slight increase in lattice parameters observed in 10Sc0.5Gd0.5CeSZ and GYBC was attributed to the small amounts of dopants. The average particle sizes of 10Sc0.5Gd0.5CeSZ and GYBC were found to be 68.7 nm and 47.3 nm, respectively, with BET surface areas of 9.7271 m^2/g and 10.5517 m^2/g, respectively, which are suitable for SOFC applications. We further investigated the XRD, cross-sectional SEM images, and EIS of LSCF-GDC cathodes at different sintering temperatures and weight ratios. As the sintering temperature increased from 1050 to 1100 °C, the electrode porosities and BET surface areas of LSCF-GDC decreased due to enhanced sintering. In the EIS analysis, it was observed that 6LSCF-4GDC exhibited lower ASR than 6.5LSCF-3.5GDC at operating temperatures of 650 °C and 700 °C. Conversely, 6.5LSCF-3.5GDC exhibited lower ASR than 6LSCF-4GDC at operating temperatures of 750 °C and 800 °C. This can be attributed to the lower ionic conductivity of LSCF at lower temperatures. A single cell composed of Ni-YSZ/10Sc0.5Gd0.5CeSZ/GYBC/6.5LSCF-3.5GDC was successfully fabricated using the sequential 3-layer co-tape casting technique. The dense 10Sc0.5Gd0.5CeSZ electrolyte and GYBC buffer layer were formed through sintering at 1250 °C and 1200 °C, respectively. The single cell demonstrated an OCV exceeding 1.0 V and a power density of 0.73 W/cm^2. Importantly, the single cell underwent a 500-h durability test without any degradation issues, indicating that 10Sc0.5Gd0.5CeSZ electrolyte and GYBC buffer layer hold promise as candidate materials for SOFCs.

Supplementary Information The online version contains supplementary material available at https://doi.org/10.1007/s40684-023-00577-6.

Acknowledgements This Research was funded and conducted under 「the Competency Development Program for Industry Specialists of Korean Ministry of Trade, Industry and Energy (MOTIE), operated by Korea Institute for Advancement of Technology(KIAT). (No. P0017120, HRD program for Foster R&D specialist of parts for eco-friendly vehicle(xEV)). This research was supported by National R&D Program through the National Research Foundation of Korea(NRF) funded by Ministry of Science and ICT(2021M3H4A3A02086497)

Data availability The datasets generated during and/or analyzed during the current study are available from the corresponding author on reasonable request.

Declarations

Conflict of Interest The authors declare that they have no conflict of interest.

References

1. Abdalla, A. M., Hossain, S., Azad, A. T., Petra, P. M. I., Begum, F., Eriksson, S. G., & Azad, A. K. (2018). Nanomaterials for solid oxide fuel cells: A review. *Renewable and Sustainable Energy Reviews, 82*, 353–368. https://doi.org/10.1016/j.rser.2017.09.046
2. Jaiswal, N., Tanwar, K., Suman, R., Kumar, D., Upadhyay, S., & Parkash, O. (2019). A brief review on ceria based solid electrolytes for solid oxide fuel cells. *Journal of Alloys and Compounds, 781*, 984–1005. https://doi.org/10.1016/j.jallcom.2018.12.015
3. Lee, K., Jin, S., Kang, J., Lee, S., & Bae, J. (2015). Development of metal supported solid oxide fuel cell based on interconnect coating. *ECS Transactions, 68*, 1721. https://doi.org/10.1149/06801.1721ecst
4. Shin, J. W., Lee, S., Go, D., Yang, B. C., Kim, T., Jo, S. E., Su, P. C., & An, J. (2023). Nanometer Yttria-doped ceria shell by atomic layer deposition over porous pt for improved oxygen reduction reactions. *International Journal of Precision Engineering and Manufacturing—Green Technology, 10*, 773–781. https://doi.org/10.1007/s40684-023-00506-7
5. Jo, M., Kim, S., & Lee, C. (2022). Morphology engineering for compact electrolyte layer of solid oxide fuel cell with roll-to-roll eco-production. *International Journal of Precision Engineering and Manufacturing—Green Technology, 9*, 431–441. https://doi.org/10.1007/s40684-022-00425-z
6. Ji, S. H., & Kim, W. J. (2022). Is coating oxide on porous metal thin-film for low-temperature solid oxide fuel cell cathode a panacea for performance enhancement? *International Journal of Precision Engineering and Manufacturing, 23*, 445–451. https://doi.org/10.1007/s12541-022-00628-z
7. Hussain, S., & Yangping, L. (2020). Review of solid oxide fuel cell materials: Cathode, anode, and electrolyte. *Energy Transitions, 4*, 113–126. https://doi.org/10.1007/s41825-020-00029-8
8. Dwivedi, S. (2020). Solid oxide fuel cell: Materials for anode, cathode and electrolyte. *International Journal of Hydrogen Energy, 45*, 23988–24013. https://doi.org/10.1016/j.ijhydene.2019.11.234
9. Sharaf, O. Z., & Orhan, M. F. (2014). An overview of fuel cell technology: Fundamentals and applications. *Renewable and Sustainable Energy Reviews, 32*, 810–853. https://doi.org/10.1016/j.rser.2014.01.012
10. Jo, S., Sharma, B., Park, D.-H., & Myung, J.-H. (2020). Materials and nano-structural processes for use in solid oxide fuel cells: A review. *Journal of the Korean Ceramic Society, 57*, 135–151. https://doi.org/10.1007/s43207-020-00022-3
11. Ji, S., Kim, W., Han, S., Jeong, S., & Park, T. (2023). Stability enhancement of reformate-fueled, low-temperature solid oxide fuel cell with nickel thin-film anode by water bubbling. *International Journal of Precision Engineering and Manufacturing— Green Technology, 10*, 999–1006. https://doi.org/10.1007/s40684-022-00484-2

12. Lee, S., Jang, Y.-H., Shin, H. Y., Lee, K., Bae, M., Kang, J., & Bae, J. (2019). Reliable sealing design of metal-based solid oxide fuel cell stacks for transportation applications. *International Journal of Hydrogen Energy, 44*, 30280–30292. https://doi.org/10.1016/j.ijhydene.2019.09.087
13. Jang, Y.-H., Lee, S., Shin, H. Y., & Bae, J. (2018). Development and evaluation of a 3-cell stack of metal-based solid oxide fuel cells fabricated via a sinter-joining method for auxiliary power unit applications. *International Journal of Hydrogen Energy, 43*, 16215–16229. https://doi.org/10.1016/j.ijhydene.2018.06.141
14. Azizi, M. A., & Brouwer, J. (2018). Progress in solid oxide fuel cell-gas turbine hybrid power systems: System design and analysis, transient operation, controls and optimization. *Applied energy, 215*, 237–289. https://doi.org/10.1016/j.apenergy.2018.01.098
15. Lee, K., Yoon, B., Kang, J., Lee, S., & Bae, J. (2017). Evaluation of Ag-doped (MnCo)3O4 spinel as a solid oxide fuel cell metallic interconnect coating material. *International Journal of Hydrogen Energy, 42*, 29511–29517. https://doi.org/10.1016/j.ijhydene.2017.10.017
16. Simwonis, D., Tietz, F., & Stöver, D. (2000). Nickel coarsening in annealed Ni/8YSZ anode substrates for solid oxide fuel cells. *Solid State Ionics, 132*, 241–251. https://doi.org/10.1016/S0167-2738(00)00650-0
17. Fan, L., Zhu, B., Su, P.-C., & He, C. (2018). Nanomaterials and technologies for low temperature solid oxide fuel cells: Recent advances, challenges and opportunities. *Nano Energy, 45*, 148–176. https://doi.org/10.1016/j.nanoen.2017.12.044
18. Yoon, B. Y., & Bae, J. (2013). Characteristics of nano La0. 6Sr0. 4Co0. 2Fe0. 8O3− δ-infiltrated La0. 8Sr0. 2Ga0. 8Mg0. 2O3− δ scaffold cathode for enhanced oxygen reduction. *International Journal of Hydrogen Energy, 38*, 13399–13407. https://doi.org/10.1016/j.ijhydene.2013.07.087
19. Yoon, B. Y., Kim, J. H., & Bae, J. (2013). Effects of infiltrated Sr and Mn doped LaCrO3 on porous La0. 8Sr0. 2Ga0. 8Mg0. 2O3-δ scaffolds used as anodes in solid oxide fuel cells. *Solid State Ionics, 249*, 26–33. https://doi.org/10.1016/j.ssi.2013.07.007
20. Kim, J., Sengodan, S., Kim, S., Kwon, O., Bu, Y., & Kim, G. (2019). Proton conducting oxides: A review of materials and applications for renewable energy conversion and storage. *Renewable and Sustainable Energy Reviews, 109*, 606–618. https://doi.org/10.1016/j.rser.2019.04.042
21. Zakaria, Z., & Kamarudin, S. K. (2021). Advanced modification of Scandia-stabilized zirconia electrolytes for solid oxide fuel cells application—a review. *International Journal of Energy Research, 45*, 4871–4887. https://doi.org/10.1002/er.6206
22. Zhigachev, A. O., Rodaev, V. V., Zhigacheva, D. V., Lyskov, N. V., & Shchukina, M. A. (2021). Doping of scandia-stabilized zirconia electrolytes for intermediate-temperature solid oxide fuel cell: A review. *Ceramics International, 47*, 32490–32504. https://doi.org/10.1016/j.ceramint.2021.08.285
23. Mahmood, A., Bano, S., Yu, J. H., & Lee, K.-H. (2015). High-performance solid oxide electrolysis cell based on ScSZ/GDC (scandia-stabilized zirconia/gadolinium-doped ceria) bi-layered electrolyte and LSCF (lanthanum strontium cobalt ferrite) oxygen electrode. *Energy, 90*, 344–350. https://doi.org/10.1016/j.energy.2015.06.109
24. Bai, B., McPhee, W. A., Smirnova, A. L., & Sammes, N. M. (2007). A comparison and characterization of CeO2-doped and Bi2O3-doped scandia stabilized zirconia as IT-SOFC electrolytes. *ECS Transactions, 7*, 2213. https://doi.org/10.1149/1.2729337
25. Lakshmi, V. V., & Bauri, R. (2011). Phase formation and ionic conductivity studies on ytterbia co-doped scandia stabilized zirconia (0.9 ZrO2–0.09 Sc2O3–0.01 Yb2O3) electrolyte for SOFCs. *Solid state sciences, 13*, 1520–1525. https://doi.org/10.1016/j.solidstatesciences.2011.05.014
26. Shin, H. C., Yu, J. H., Lim, K. T., Lee, H. L., & Baik, K. H. (2016). Effects of Partial Substitution of CeO 2 with M 2 O 3 (M= Yb, Gd, Sm) on Electrical Degradation of Sc 2 O 3 and CeO 2 Co-doped ZrO 2. *Journal of the Korean Ceramic Society, 53*, 500–505. https://doi.org/10.4191/kcers.2016.53.5.500
27. Arachi, Y., Asai, T., Yamamoto, O., Takeda, Y., Imanishi, N., Kawate, K., & Tamakoshi, C. (2001). Electrical conductivity of ZrO2 Sc2 O 3 doped with HfO2, CeO2, and Ga2 O 3. *Journal of the Electrochemical Society, 148*, A520. https://doi.org/10.1149/1.1366622
28. Wang, Z., Cheng, M., Bi, Z., Dong, Y., Zhang, H., Zhang, J., Feng, Z., & Li, C. (2005). Structure and impedance of ZrO2 doped with Sc2O3 and CeO2. *Materials Letters, 59*, 2579–2582. https://doi.org/10.1016/j.matlet.2004.07.065
29. Shimazu, M., Isobe, T., Ando, S., Hiwatashi, K.-I., Ueno, A., Yamaji, K., Kishimoto, H., Yokokawa, H., Nakajima, A., & Okada, K. (2011). Stability of Sc2O3 and CeO2 co-doped ZrO2 electrolyte during the operation of solid oxide fuel cells. *Solid State Ionics, 182*, 120–126. https://doi.org/10.1016/j.ssi.2010.08.030
30. Zhigachev, A. O., Zhigacheva, D. V., & Lyskov, N. V. (2019). Influence of yttria and ytterbia doping on phase stability and ionic conductivity of ScSZ solid electrolytes. *Materials Research Express, 6*, 105534. https://doi.org/10.1088/2053-1591/ab3ed0
31. Haering, C., Roosen, A., Schichl, H., & Schnöller, M. (2005). Degradation of the electrical conductivity in stabilised zirconia system: Part II: Scandia-stabilised zirconia. *Solid State Ionics, 176*, 261–268. https://doi.org/10.1016/j.ssi.2004.07.039
32. Yamaji, K., Kishimoto, H., Brito, M. E., Horita, T., Yokokawa, H., Shimazu, M., Yashiro, K., Kawada, T., & Mizusaki, J. (2013). Effect of Mn-doping on stability of Scandia stabilized zirconia electrolyte under dual atmosphere of solid oxide fuel cells. *Solid State Ionics, 247*, 102–107. https://doi.org/10.1016/j.ssi.2013.05.019
33. Lim, K. T., Lee, H. L., Shin, H. C., Lee, C. H., & Kim, B. S. (2017). Highly ionic conductive zirconia electrolyte for high-efficiency solid oxide fuel cell. *US patent, 9*(847), 545.
34. Lee, S., Lee, K., Jang, Y.-H., & Bae, J. (2017). Fabrication of solid oxide fuel cells (SOFCs) by solvent-controlled co-tape casting technique. *International Journal of Hydrogen Energy, 42*, 1648–1660. https://doi.org/10.1016/j.ijhydene.2016.07.066
35. Kang, S., Lee, J., Cho, G. Y., Kim, Y., Lee, S., Cha, S. W., & Bae, J. (2020). Scalable fabrication process of thin-film solid oxide fuel cells with an anode functional layer design and a sputtered electrolyte. *International Journal of Hydrogen Energy, 45*, 33980–33992. https://doi.org/10.1016/j.ijhydene.2020.09.033
36. Lee, K., Kang, J., Lee, J., Lee, S., & Bae, J. (2018). Evaluation of metal-supported solid oxide fuel cells (MS-SOFCs) fabricated at low temperature (~ 1000 °C) using wet chemical coating processes and a catalyst wet impregnation method. *International Journal of Hydrogen Energy, 43*, 3786–3796. https://doi.org/10.1016/j.ijhydene.2018.01.027
37. Lim, Y. H., Lee, J., Yoon, J. S., Kim, C. E., & Hwang, H. J. (2007). Electrochemical performance of Ba0. 5Sr0. 5CoxFe1− xO3− δ (x= 0.2–0.8) cathode on a ScSZ electrolyte for intermediate temperature SOFCs. *Journal of power sources, 171*, 79–85. https://doi.org/10.1016/j.jpowsour.2007.05.050
38. Loureiro, F. J., Yang, T., Stroppa, D. G., & Fagg, D. P. (2015). Pr 2 O 2 SO 4–La 0.6 Sr 0.4 Co 0.2 Fe 0.8 O 3−δ: A new category of composite cathode for intermediate temperature-solid oxide fuel cells. *Journal of Materials Chemistry A, 3*, 12636–12641. https://doi.org/10.1039/C4TA06640E
39. Kim, W.-H., Song, H.-S., Moon, J., & Lee, H.-W. (2006). Intermediate temperature solid oxide fuel cell using (La, Sr)(Co, Fe) O3-based cathodes. *Solid State Ionics, 177*, 3211–3216. https://doi.org/10.1016/j.ssi.2006.07.049

40. Hsieh, W.-S., Lin, P., & Wang, S.-F. (2014). Characteristics of electrolyte supported micro-tubular solid oxide fuel cells with GDC-ScSZ bilayer electrolyte. *International Journal of Hydrogen Energy, 39*, 17267–17274. https://doi.org/10.1016/j.ijhydene.2014.08.060
41. Rehman, S. U., Shaur, A., Kim, H. S., Joh, D. W., Song, R. H., Lim, T. H., Hong, J. E., Park, S. J., & Lee, S. B. (2021). Effect of transition metal doping on the sintering and electrochemical properties of GDC buffer layer in SOFCs. *International Journal of Applied Ceramic Technology, 18*, 511–524. https://doi.org/10.1111/ijac.13650
42. Accardo, G., Frattini, D., Ham, H., Han, J., & Yoon, S. (2018). Improved microstructure and sintering temperature of bismuth nano-doped GDC powders synthesized by direct sol-gel combustion. *Ceramics International, 44*, 3800–3809. https://doi.org/10.1016/j.ceramint.2017.11.165
43. Gil, V., Tartaj, J., Moure, C., & Duran, P. (2007). Rapid densification by using Bi2O3 as an aid for sintering of gadolinia-doped ceria ceramics. *Ceramics International, 33*, 471–475. https://doi.org/10.1016/j.ceramint.2005.10.012
44. Lim, K. T., Lee, H. L., Shin, H. C., Lee, C. H., Kim, B. S., Choi, J. H., & Lee, S. J. (2020). Ceria electrolyte for low-temperature sintering and solid oxide fuel cell using the same. *US patent, 10*(581), 102.
45. Fujimori, H., Yashima, M., Kakihana, M., & Yoshimura, M. (1998). Structural changes of scandia-doped zirconia solid solutions: Rietveld analysis and Raman scattering. *Journal of the American Ceramic Society, 81*, 2885–2893. https://doi.org/10.1111/j.1151-2916.1998.tb02710.x
46. Li, J., Li, J.-G., Liu, S., Li, X., Sun, X., & Sakka, Y. (2013). The development of Ce3+-activated (Gd, Lu) 3Al5O12 garnet solid solutions as efficient yellow-emitting phosphors. *Science and Technology of Advanced Materials*. https://doi.org/10.1088/1468-6996/14/5/054201
47. Vinothkumar, G., Rengaraj, S., Arunkumar, P., Cha, S. W., & Suresh Babu, K. (2018). Ionic radii and concentration dependency of RE3+ (Eu3+, Nd3+, Pr3+, and La3+)-doped cerium oxide nanoparticles for enhanced multienzyme-mimetic and hydroxyl radical scavenging activity. *The Journal of Physical Chemistry C, 123*, 541–553. https://doi.org/10.1021/acs.jpcc.8b10108
48. Shannon, R. D. (1976). Revised effective ionic radii and systematic studies of interatomic distances in halides and chalcogenides. *Acta crystallographica section A: Crystal physics, diffraction, theoretical and general crystallography, 32*, 751–767. https://doi.org/10.1107/S0567739476001551
49. Shojaie, A. F., & Loghmani, M. H. (2010). La3+ and Zr4+ co-doped anatase nano TiO2 by sol-microwave method. *Chemical Engineering Journal, 157*, 263–269. https://doi.org/10.1016/j.cej.2009.12.025
50. Ahuja, A., Gautam, M., Sinha, A., Sharma, J., Patro, P., & Venkatasubramanian, A. (2020). Effect of processing route on the properties of LSCF-based composite cathode for IT-SOFC. *Bulletin of Materials Science, 43*, 1–9. https://doi.org/10.1007/s12034-020-2075-y
51. Raju, K., Kim, S., Yu, J. H., Kim, S.-H., Seong, Y.-H., & Han, I.-S. (2018). Rietveld refinement and estimation of residual stress in GDC–LSCF oxygen transport membrane ceramic composites. *Ceramics International, 44*, 10293–10298. https://doi.org/10.1016/j.ceramint.2018.03.036
52. Kim, Y.-M., Kim-Lohsoontorn, P., Baek, S.-W., & Bae, J. (2011). Electrochemical performance of unsintered Ba0.5Sr0.5Co0.8Fe0.2O3−δ, La0.6Sr0.4Co0.8Fe0.2O3−δ, and La0.8Sr0.2MnO3−δ cathodes for metal-supported solid oxide fuel cells. *International Journal of Hydrogen Energy, 36*, 3138–3146. https://doi.org/10.1016/j.ijhydene.2010.10.065
53. Zhang, J., Ji, Y., Gao, H., He, T., & Liu, J. (2005). Composite cathode La0.6Sr0.4Co0.2Fe0.8O3–Sm0.1Ce0.9O1.95–Ag for intermediate-temperature solid oxide fuel cells. *Journal of Alloys and Compounds, 395*, 322–325. https://doi.org/10.1016/j.jallcom.2004.11.056
54. Li, N., Verma, A., Singh, P., & Kim, J.-H. (2013). Characterization of La0.58Sr0.4Co0.2Fe0.8O3−δ–Ce0.8Gd0.2O2 composite cathode for intermediate temperature solid oxide fuel cells. *Ceramics International, 39*, 529–538. https://doi.org/10.1016/j.ceramint.2012.06.059
55. Khurana, S., Johnson, S., Karimaghaloo, A., & Lee, M. H. (2018). Effect of Sintering process with Co 3 O 4 on the performance of LSCF-based cathodes for solid oxide fuel cells. *International Journal of Precision Engineering and Manufacturing-Green Technology, 5*, 637–642. https://doi.org/10.1007/s40684-018-0066-x
56. Jiang, S. P. (2019). Development of lanthanum strontium cobalt ferrite perovskite electrodes of solid oxide fuel cells-A review. *International Journal of Hydrogen Energy, 44*, 7448–7493. https://doi.org/10.1016/j.ijhydene.2019.01.212
57. Abd Aziz, A. J., Baharuddin, N. A., Somalu, M. R., & Muchtar, A. (2020). Review of composite cathodes for intermediate-temperature solid oxide fuel cell applications. *Ceramics International, 46*, 23314–23325. https://doi.org/10.1016/j.ceramint.2020.06.176
58. Shearing, P., Bradley, R., Gelb, J., Tariq, F., Withers, P., & Brandon, N. (2012). Exploring microstructural changes associated with oxidation in Ni–YSZ SOFC electrodes using high resolution X-ray computed tomography. *Solid State Ionics, 216*, 69–72. https://doi.org/10.1016/j.ssi.2011.10.015
59. Sarikaya, A., Petrovsky, V., & Dogan, F. (2013). Development of the anode pore structure and its effects on the performance of solid oxide fuel cells. *International Journal of Hydrogen Energy, 38*, 10081–10091. https://doi.org/10.1016/j.ijhydene.2013.05.160
60. Wright, G. J., & Yeomans, J. A. (2008). Constrained sintering of yttria-stabilized zirconia electrolytes: The influence of two-step sintering profiles on microstructure and gas permeance. *International Journal of Applied Ceramic Technology, 5*, 589–596. https://doi.org/10.1111/j.1744-7402.2008.02263.x
61. Teocoli, F., Ni, D. W., Brodersen, K., Foghmoes, S. P. V., Ramousse, S., & Esposito, V. (2014). Effects of co-sintering in self-standing CGO/YSZ and CGO/ScYSZ dense bi-layers. *Journal of Materials science, 49*, 5324–5333. https://doi.org/10.1007/s10853-014-8235-y
62. Haanappel, V. A. C., Mai, A., & Mertens, J. (2006). Electrode activation of anode-supported SOFCs with LSM- or LSCF-type cathodes. *Solid State Ionics, 177*, 2033–2037. https://doi.org/10.1016/j.ssi.2005.12.038
63. Simner, S. P., Anderson, M. D., Pederson, L. R., & Stevenson, J. W. (2005). Performance variability of La (Sr) FeO3 SOFC cathode with Pt, Ag, and Au current collectors. *Journal of the Electrochemical Society, 152*, A1851. https://doi.org/10.1149/1.1995687
64. Shin, S. M., Yoon, B. Y., Kim, J. H., & Bae, J. M. (2013). Performance improvement by metal deposition at the cathode active site in solid oxide fuel cells. *International Journal of Hydrogen Energy, 38*, 8954–8964. https://doi.org/10.1016/j.ijhydene.2013.04.115
65. Song, J.-H., Jung, M. G., Park, H. W., & Lim, H.-T. (2013). The effect of fabrication conditions for GDC buffer layer on electrochemical performance of solid oxide fuel cells. *Nano-Micro Letters, 5*, 151–158. https://doi.org/10.1007/BF03353744
66. Khan, M. Z., Mehran, M. T., Song, R.-H., Lee, J.-W., Lee, S.-B., Lim, T.-H., & Park, S.-J. (2016). Effect of GDC interlayer thickness on durability of solid oxide fuel cell cathode. *Ceramics International, 42*, 6978–6984. https://doi.org/10.1016/j.ceramint.2016.01.085

Sanghun Lee is an Assistant Professor in the Department of Climate and Energy Systems Engineering at Ewha Womans University, South Korea. He has received his Ph.D. from Korea Advanced Institute of Science and Technology (KAIST). He also worked as a Postdoctoral Researcher at National Renewable Energy Lab (NREL) in US. His main research interests are technoeconomic analysis, lifecycle assessment, chemical process simulation, and fundamental research on electrolyzers, fuel cells and hydrogen storages.

Kunho Lee is a Researcher at Saudi Aramco. He has received his Ph.D. from Korea Advanced Institute of Science and Technology (KAIST). His main research interests are solid oxide fuel cells and hydrogen energy.

Jaemyung Lee is a Senior Research Engineer at Hyundai Motors Company. He has received his Ph.D. from Korea Advanced Institute of Science and Technology (KAIST). His main research interest is developing an fuel reforming system for hydrogen production.

Jaeseok Lee is a Ph.D. candidate at Korea Advanced Institute of Science and Technology (KAIST). His main research interests are metal-suppoted solid oxide fuel cells.

Taehong Kim is a Ph.D. candidate at Korea Advanced Institute of Science and Technology (KAIST). His main research interests are solid oxide fuel cells with various fuels.

Joongmyeon Bae is a Professor in the Department of Mechanical Engineering at Korea Advanced Institute of Science and Technology (KAIST). He has received his Ph.D. from Imperial College. He also worked as a Researcher at Electrotechnical Laboratory (ETL) in Japan and Senior Researcher at Argonne National Lab. in US. His main research interests are solid oxide fuel cells, electrolyzers, reforming, and hydrogen energy system developments.